EUROPEAN ORGANISATION FOR NUCLEAR RESEARCH

CERN-EP/88-45
April 6th, 1988

Direct Photon Production at the CERN Proton-Antiproton Collider.

UA1 Collaboration, CERN, Geneva, Switzerland

Aachen[1] - Amsterdam (NIKHEF)[2] - Annecy (LAPP)[3] - Birmingham[4] - CERN[5] - Harvard[6] - Helsinki[7] - Kiel[8] - Imperial College, London[9] - Queen Mary College, London[10] - Madrid (CIEMAT)[11] - MIT[12] - Padua[13] - Paris (College de France)[14] - Riverside[15] - Rome[16] - Rutherford Appleton Lab[17] - Saclay (CEN)[18] - Victoria[19] - Vienna[20] - Wisconsin[21] Collaboration

C. Albajar[5], M.G. Albrow[17], O.C. Allkofer[8], A. Astbury[19], B. Aubert[3], T. Axon[9], C. Bacci[16], T. Bacon[9], N. Bains[4], J. R. Batley[10], G. Bauer[6], S. Beingessner[19], A. Bettini[13], A. Bezaguet[5], R. Bonino[4], K. Bos[2], E. Buckley[6], G. Busetto[13], P. Catz[3], P. Cennini[5], S. Centro[13], F. Ceradini[16], D.G. Charlton[4], G. Ciapetti[16], S. Cittolin[5], D. Clarke[10], D. Cline[21], C. Cochet[18], J. Colas[3], P. Colas[18], M. Corden[4], J.A. Coughlan[17], G. Cox[4], D. Dau[8], J.P. deBrion[18], M. DeGiorgi[13], M. Della Negra[5], M. Demoulin[5], D. Denegri[5,18], A. DiCiaccio[5,16], F.J. Diez Hedo[11], L. Dobrzynski[14], J. Dorenbosch[2], J. D. Dowell[4], E. Duchovni[5], K. Eggert[1], E. Eisenhandler[10], N. Ellis[4], P. Erhard[1], H. Faissner[1], I.F. Fensome[10], A. Ferrando[11], M. Finćke-Keeler[19], P. Flynn[17], G. Fontaine[14], J. Garvey[4], D. Gee[15], S. Geer[6], A. Geiser[1], C. Ghesquiere[14], P. Ghez[3], C. Ghiglino[3], Y. Giraud-Heraud[14], A. Givernaud[5,18], A. Gonidec[5], H. Grassmann[1], J.M. Gregory[4], W. Haynes[17], S.J. Haywood[4], D.J. Holthuizen[2], M. Ikeda[15], W. Jank[5], M. Jimack[4], G. Jorat[5], D. Joyce[15], P.I.P. Kalmus[10], V. Karimäki[7], R. Keeler[19], I. Kenyon[4], A. Kernan[15], A. Khan[9], W. Kienzle[5], R. Kinnunen[7], M. Krammer[20], J. Kroll[6], D. Kryn[14], F. Lacava[16], M. Landon[10], J.P. Lees[3], R. Leuchs[8], S. Levegrün[8], S. Li[19], M. Lindgren[15], D. Linglin[3], P. Lipa[20], E. Locci[5], T. Markiewicz[21], C. Markou[9], M. Markytan[20], M.A. Marquina[11], G. Maurin[5], J.-P. Mendiburu[14], A. Meneguzzo[13], J. P. Merlo[15], T. Meyer[5], M.-N. Minard[3], M. Mohammadi[21], K. Morgan[15], H.-G. Moser[1], A. Moulin[1], B. Mours[3], Th. Muller[5], L. Naumann[5], P. Nedelec[14], A. Nisati[16], A. Norton[5], F. Pauss[5], C. Perault[3], E. Petrolo[16], G. Piano Mortari[16], E. Pietarinen[7], C. Pigot[18], M. Pimiä[7], A. Placci[5], J.-P. Porte[5], M. Preischl[8], E. Radermacher[5], T. Redelberger[1], H. Reithler[1], J.-P. Revol[12], D. Robinson[9], T. Rodrigo[11], J. Rohlf[6], C. Rubbia[5], G. Sajot[14], G. Salvini[16], J. Sass[5], D. Samyn[5], D. Schinzel[5], M. Schröder[8], A. Schwartz[6], W. Scott[17], C. Seez[9], T. P. Shah[17], I. Sheer[15], I. Siotis[9], D. Smith[15], R. Sobie[19], P. Sphicas[12], J. Strauss[20], J. Streets[4], C. Stubenrauch[18], D. Summers[21], K. Sumorok[6], F. Szoncso[20], C. Tao[14], A. Taurok[20], I. ten Have[2], S. Tether[12], G. Thompson[10], E. Tscheslog[1], J. Tuominiemi[7], W. van de Guchte[2], A. van Dijk[2], B. van Eijk[2], J.P. Vialle[3], L. Villasenor[21], T.S. Virdee[9], W. von Schlippe[10], J. Vrana[14], V. Vuillemin[5], K. Wacker[1], G. Walzel[20], A. Wildish[9], I. Wingerter[3], S. J. Wimpenny[5], X. Wu[12], C.-E. Wulz[20], T. Wyatt[5], M. Yvert[3], C. Zaccardelli[16], I. Zacharov[2], N. Zaganidis[18], L. Zanello[16] and P. Zotto[13].

(Submitted to Physics Letters B)

Abstract

Isolated photons, produced directly by a hard scattering process, have been observed in the UA1 experiment at the CERN $p\bar{p}$ collider at centre-of-mass energies $\sqrt{s}$=546 GeV and $\sqrt{s}$=630 GeV. Single and double photon differential cross-sections have been determined and found to be consistent with the expectations of QCD.

Introduction

The study of direct production of photons is a clean test of QCD, because knowledge of the outgoing particle requires no input from non-perturbative theory, and because full predictions are available to order α_s^2. In spite of the large background coming from π^0 and other neutral mesons, several experiments [1] have shown clear signals in agreement with calculations based on QCD. Unfortunately, rejection of the π^0 background by the separate detection of the two decay photons is impossible with the granularity of the present UA1 calorimeters because their mean opening angle is too small. Nevertheless, we can take advantage of the fact that high transverse energy π^0's commonly appear as part of a jet and are therefore not isolated as would be expected for a photon produced directly in the hard scattering process.

In this paper, we first describe the apparatus and the data sample. Then the extraction of the direct photon signal is considered. This is done on a statistical basis using information from the isolation of the photon candidate and the pattern of the longitudinal energy deposition of the electromagnetic shower. We present the single, isolated, photon differential cross-section measured at $\sqrt{s}$=546 GeV and $\sqrt{s}$=630 GeV, at high photon transverse energy, E_{T}^{γ}, (16 GeV $< E_T^{\gamma} <$ 100 GeV), in the pseudo-rapidity range $|\eta| < 3$. We also give results on the event topology, the angular distribution of photons, and on the two photon cross-section.

Apparatus and Trigger

The UA1 detector and trigger conditions are those used for W/Z studies, and we refer the reader to reference [2] for more details. Photons are detected by lead-scintillator calorimeters ('gondolas' for $|\eta| < 1.5$ and 'bouchons' for $1.5 < |\eta| < 3$). Each has a depth of at least 27 radiation lengths, which is sufficient to contain fully the highly energetic electromagnetic showers considered in this analysis. Energy resolution is approximately $\sigma(E) = 0.16\sqrt{E}$, where E is in GeV. An outer iron-scintillator calorimeter, constituting a minimum of 5 interaction lengths, is used to confirm the electromagnetic character of the shower. Charged tracks are measured by the central detector, a large volume drift chamber surrounding the interaction point and operated in a homogeneous 0.7 T magnetic field. These detectors cover a very large solid angle. Small areas of inefficiency, in the vertical plane (azimuthal angle within 15^0 of the vertical) and in the gondola-bouchon interface ($1.4 < |\eta| < 1.6$), are removed from the study.

This analysis [3] uses data collected during the 1983 collider run at $\sqrt{s} = 546$ GeV ($\int L\mathrm{dt}$=118 nb^{-1}), and during 1984 and 1985 runs at $\sqrt{s}$ =630 GeV ($\int L\mathrm{dt}$=567 nb^{-1}). The first level trigger is the 'electromagnetic trigger' which selects clusters of two adjacent gondola or bouchon calorimeter cells having a transverse energy, E_{T}, in excess of 10 GeV. The second level trigger applies a higher threshold on a more precise reconstruction of the energy. The luminosity and thresholds used in this analysis are given in Table 1. The second level trigger additionally uses an energy-isolation criterion for all 1983 and 1984

data and for candidate clusters with transverse energy less than 15 GeV in the 1985 data. This isolation criterion is based on the transverse energy deposited within a cone of radius R=$\sqrt{(\Delta\eta)^2 + (\Delta\phi)^2}$=0.4 ($\phi$ being the azimuthal angle measured in radians) *around* the cluster. For the lead-scintillator (so-called, 'electromagnetic') calorimeters this is required to be less than 5% of the cluster transverse energy, whereas for the total calorimetry (including the iron-scintillator, or, 'hadron' calorimeter) it should be below 10%.

In parallel with the single cluster trigger, a 'two photon' trigger is applied with lower thresholds (also given in Table 1) for 1984 and 1985 data. The second level trigger for the two photon analysis requires isolation criteria, as describe above, to be applied to each candidate separately.

Analysis

In the final reconstruction of each event, measured energies are corrected for known ageing effects of the calorimeters. A selection is then made to remove instrumental background and retain events containing isolated neutral electromagnetic clusters of large transverse energy. Without this selection the data sample would be dominated by the principle source of background which is fluctuations of narrow jets fragmenting into π^0's (mainly one π^0). The selection demands:

- a cluster in the electromagnetic calorimeter consistent with a single electromagnetic shower of transverse energy above a given threshold (see Table 1).
- small transverse component of 'missing' energy. This requirement is made to suppress triggers arising from cosmic rays and beam halo background, and also removes some instrumental problems. Missing transverse energy, $E_{\rm T}^{miss}$, is defined as the magnitude of the vector sum of transverse energy flows. Calorimeter response fluctuations give an r.m.s. spread in $E_{\rm T}^{miss}$ which can be well parametrised by $\sigma = 0.7\sqrt{E_{\rm T}}$ where $E_{\rm T}$ is the *total* transverse energy in GeV, *i.e* the scalar sum of the transverse energies deposited in all calorimeter cells. We require $E_{\rm T}^{miss}$ to be less than 2.5 σ.
- charged track isolation of the clusters in order to favour neutral clusters over hadronic jets. We sum the transverse momenta of the charged tracks detected in the central detector in a cone of radius R=0.7 around the cluster and demand that the magnitude of this quantity ($\sum p_{\rm T}$) is less than both 2 GeV and 10% of the cluster transverse energy.
- calorimeter energy isolation of the clusters in order to further reject jets. We demand that the magnitude of the sum of the *additional* transverse energy ($\sum E_{\rm T}$) measured in a cone of radius R=0.7 around the cluster is less than both 2 GeV and 10% of the cluster transverse energy.

The following analysis is then performed separately in three pseudo-rapidity ranges: (i) $|\eta| < 0.8$, the central region of the gondolas where photons are incident almost normally on the calorimeter cells, (ii) $0.8 < |\eta| < 1.4$, the gondola region with a larger angle of incidence, and (iii) $1.6 < |\eta| < 3$, the bouchon region where, again, photons are incident almost normally.

Determination of single photon contribution

We now describe the calculation of the contribution of single, direct, photons in the sub-sample of clusters with $E_{\rm T} > 20$ GeV. This sample contains 3684 events. To determine the fraction of direct photon events in this sample, F_γ, we utilise the expected differences,

in both production and detection, between direct photons and π^0's or other neutral mesons.

For production differences, we refine the concept of cluster isolation and we increase the size of the cone to that more typical of the size of a jet. We define:

$$E_c = max\left(\sum_{R=0}^{0.7} E_{\rm T}, \sum_{R=0}^{0.7} p_{\rm T}\right) \text{ and } E_r = max\left(\sum_{R=0.7}^{1} E_{\rm T}, \sum_{R=0.7}^{1} p_{\rm T}\right)$$

E_c represents the transverse energy in a cone of radius 0.7 around the γ/π^0 candidate, excluding the γ/π^0 energy itself. E_r is a measure of the *additional* transverse energy deposited in an ring around the γ/π^0 candidate with a internal radius of 0.7 and an external radius of 1 in (η, ϕ) space. For direct photon production, both E_c and E_r are expected to be small as they arise only from contributions of the spectator system or of gluons radiated from the colliding partons (underlying event). In π^0 production, however, they both additionally contain fragments of the accompanying jet and final state bremsstrahlung. The distributions of E_c and E_r are thus expected to extend to higher values.

Differences in the detection properties of π^0's and γ's are exemplified by the pattern of the longitudinal energy deposition of the shower. The electromagnetic calorimeter is segmented in depth into four read out 'samplings'. At normal incidence, the first sampling comprises 3.3 radiation lengths. The energy deposition in this first sampling, S_1, is expected to be greater for a π^0 than for a single photon of the same energy, since the decay photons from the π^0 have lower individual energies, and therefore smaller penetration in the calorimeter. The fraction of energy deposited in the first sampling, S_1/E, should reflect this difference.

The distributions of the three variables $E_c, E_r, S_1/E$ for the data sample $E_{\rm T} > 20$ GeV and $|\eta| < 0.8$ (1353 events) are shown in figures 1a,1b and 1c. The E_c distribution does not extend beyond 2 GeV because of the selection cuts, but the *shape* of the distribution is independent of the selection. The distribution of E_r is a completely independent measurement of isolation. A peak is observed at very small values of E_c and E_r, suggestive of direct photon production. The S_1/E variable has a broad distribution peaking near $\approx 5\%$ and extending up to 20%.

In order to make a statistical assessment of F_γ, we now determine the expected distributions in figures 1a,1b for *pure* samples of π^0 and of direct photons. For the former case we use the two-parton hard scatter ISAJET Monte Carlo [4], with full simulation of the UA1 detector. Events are generated, then reconstructed and selected in an identical manner as real data. The parameters of the Monte Carlo which control jet fragmentation and spectator activity have been tuned to give agreement with UA1 data on jet shapes. We note however that our method to separate isolated photons from π^0's background relies mainly on the assumption that there exist no physics source of isolated π^0's.

By analogy with W/Z production [5], we have assumed that the transverse energy flow in direct photon events, other than the photon and the recoiling jet, is similar to that in minimum bias events. We have therefore used our minimum bias data to determine the E_c and E_r distributions in the photon case. To get pure samples of background π^0 or of direct photons for comparison with the S_1/E distribution, we rely on detailed simulations of electromagnetic showers in calorimeter cells with the Monte Carlo program GEANT [6]. These simulations include multi-π^0 effects, using ISAJET information, for the case of shower behaviour of jets.

Having obtained the behaviour of pure samples in this way, the three data distributions in E_c, E_r and in S_1/E were fitted in each of the three pseudo-rapidity ranges to yield

independent assessments of F_γ, the fraction of direct photon events. A priori, the F_γ values could be different for the three pseudo-rapidity ranges. The results are given in Table 2. The quoted statistical errors arise from the fits and the systematic errors allow for uncertainties in the determination of the pure π^0/γ distributions. They are estimated by:

- comparing the transverse energy flow of minimum bias events with photon candidates for the measurements of isolation.
- fluctuating the E_c, E_r values of π^0 (jet) Monte Carlo events by $\pm 5\%$.
- Varying the parameters of GEANT that control the S_1/E ratio such that the result for electrons in generated W and Z events still agrees with the corresponding distributions from real W and Z events.

In figure 1 we show as a typical example the resulting fitted distributions for the region $E_{\rm T}^\gamma$>20 GeV, $|\eta| < 0.8$, together with the two separate contributions, fitted independently for each figure. A clear signal is observed for direct photon production.

The results of Table 2 indicate that within each pseudo-rapidity range, the three independent determinations are consistent. To condense the information from these three variables, we define a new one by:

$$L_\gamma = ln(P_{E_c} \times P_{E_r} \times P_{S_1/E})$$

where the P_i are the direct photon Monte Carlo distributions ($i = E_c,\ E_r,\ S_1/E$). The results of a two component fit to the L_γ distribution for the same data sample are given in Table 2 and figure 1d. As expected, the values of F_γ so obtained are consistent with the independent fits, but with smaller errors.

Direct single photon cross-section

The direct photon cross-section calculation is based on the selection criteria described above with the additional requirement of a positive value of L_γ, to further enrich the sample, and with slightly different thresholds (see table 1). This gives a total of 2350 events.

The direct photon sample still contains a background contribution from π^0's. The efficiency for detecting the soft fragments near to a π^0 should improve with increasing energy, and therefore F_γ should increase with $E_{\rm T}^\gamma$. F_γ has been determined by fitting the L_γ distribution in several bins of $E_{\rm T}^\gamma$, assuming a function of the form $\{1+{\rm Aexp}(-{\rm B}E_{\rm T})\}^{-1}$, where A and B are fitted parameters. Independent results at $\sqrt{s} = 630$GeV for pseudo-rapidity interval $|\eta| < 0.8$ and $0.8 < |\eta| < 1.4$ are shown in Fig. 2, where hatched areas represents the systematic errors. As expected, we note a tendency towards purer samples at higher transverse energies. Because of limited statistics, the $E_{\rm T}$ dependence of F_γ for the interval $1.6 < |\eta| < 3$ has been taken from the preceding interval and only the normalisation has been fitted. Likewise the $E_{\rm T}$ dependence of F_γ at $\sqrt{s} = 630$GeV has been used to analyse the data at $\sqrt{s} = 546$GeV.

There then follow corrections for geometrical acceptance (83%), for selection efficiencies ($\approx 55\%$), and for the smearing effect of finite energy resolution in the $E_{\rm T}^\gamma$ spectrum ($\approx 1\%$ corrections). The final cross-sections, adjusted further to apply at the centre of each ($E_{\rm T}^\gamma$,η) bin, are given in Table 3. The systematic errors here correspond only to the background correction. In addition, there is an overall uncertainty of 23% arising from lack of knowledge of the luminosity (15%), calibration of the calorimeter (3% on the energy scale inducing a 16% uncertainty on the cross-section) and inefficiencies (8%).

In figure 3, the results are compared to order α_s^2 QCD inclusive cross-sections from reference [7] †) (dashed line). Since we apply isolation criteria, it is more relevant to compare our result to a cross-section for isolated photons (full line). It is computed by excluding all quark photon bremsstrahlung with quark-photon angles less than 57^0, which corresponds to R=1 for $\eta = 0$. This cross-section for isolated photons is in good agreement with our data. Because of the high transverse energy, the theoretical expectations are only weakly sensitive to choices of the structure function, energy scale and value of the QCD scale parameter Λ. Typically the uncertainty on the calculated cross-section is of the order of 20 % making the comparison to our data a strong test of QCD.

Topology of direct photon events

We can now go further and take advantage of the full UA1 detector to study the topology of the direct photon events.

Both the Compton ($gq \rightarrow q\gamma$) and the annihilation ($q\bar{q} \rightarrow g\gamma$) Born term graphs, predict that direct photons are produced azimuthally opposite to a *single* parton which is detected as a jet, where for our purposes a jet is defined by the UA1 jet-finding algorithm [10]. This algorithm combines calorimeter hits within a cone of radius R=1 around the highest transverse energy hit. Corrections are applied to the energy and momentum of each jet mainly to account for the energy loss outside the cone, on the basis of a Monte Carlo simulation using ISAJET [4].

All photon candidate events contain at least one jet. The jet with the highest transverse energy is back-to-back in azimuth to the photon as shown in figure 4; its energy is similar to the energy of the photon. Of the direct photon events with $E_T > 20$ GeV, $11 \pm 1\%$ contain a second jet with transverse energy greater than 15 GeV. This fraction is identical to the ratio two-jets/three-jets in π^0 events (the π^0 sample consists of all events which pass the same selection criteria as the direct photon sample, except the L_γ cut). A study of photon-jet mass distributions or of photon-two-jet mass distributions does not show any special behaviour.

We can study the dynamics of the photon-jet system in single-jet events. The most sensitive variable is the $\cos\theta^*$ distribution where θ^* is the angle of the photon relative to the mean beam axis in the photon-jet centre-of-mass (Collins-Soper definition). To first order, we expect a $(1\text{-}\cos\theta^*)^{-1}$ distribution for direct photon events and a $(1\text{-}\cos\theta^*)^{-2}$ distribution for π^0 (jet) events [11]. It is convenient to take the ratio of these two distributions, since we measure direct photon and π^0 (jet) at the same time and consequently no acceptance correction is needed. To have a more homogeneous sample we consider only clusters with $E_T > 20$ GeV taken at $\sqrt{s} = 630$ GeV. The direct photon sample, estimated to be $65 \pm 2.5 \pm 6\%$ pure in direct photon events, is the one used to compute the cross-section. The corresponding π^0 sample is estimated to be $89 \pm 0.5 \pm 1\%$ pure in background events. Figure 5 shows the ratio of the two distributions for events with $|\eta_\gamma| < 0.8$, which is the range where we have the best separation between direct photons and π^0 . An increase of the ratio is observed, consistent with the expectation (solid line) if we take into account the residual contamination of the two samples.

We have also studied the underlying event for the direct photon sample and for the

†) These are cross-sections computed with the set I structure functions of Duke and Owens [8] in the so called 'optimised scale scheme'[9], a choice which minimises the variation of the cross-section as a function of the scale.

π^0 sample. This study shows that the outlying transverse energy flow can be represented as a constant quantity plus an amount equal to the transverse momentum of the system formed by the photon and the recoiling jet. If this transverse momentum is not negligible, it is balanced by a second jet. The constant quantity is interpreted as a measure of the transverse momentum activity of the underlying event. Since we know the fraction of direct photons in both sample, we can estimate the activity of the underlying event for *pure* direct photon events. This activity is consistent with the transverse energy flow in minimum bias events. A posteriori, this is a justification of the use of the minimum bias events, in the previous sections, to compute the expected distribution for pure direct photon events.

Two-photon cross-section

In the sample of events with two electromagnetic clusters which were taken in 1984 and 1985 we have looked for two-photon candidates. We use the same selection criteria as for the single photon analysis except that the transverse energy thresholds are set to 12 GeV for the final selection. We found six candidates. Their individual characteristics are given in Table 4. These events contain just two-photon candidates back-to-back in azimuth with balanced energy, in addition to the background activity as expected for QCD production. There is an expectation of 0.9±0.45 events which come from two-jet events or from single-photon+jet events where the fragmentation of the jet yields one or more π^0. This number is computed using the observed rate of π^0 production. After background subtraction, acceptance and efficiency corrections, the integrated two-photon cross-section in $p\bar{p}$ collision at $\sqrt{s}$=630 GeV is

$$\sigma_{\gamma\gamma} = 38 \pm 19 \pm 10 \text{ pb for } E_{T\gamma} > 12 \text{ GeV and } |\eta| < 3.$$

For a comparison with the QCD prediction to order α_s^2 [12] we need yet another cut since this prediction is expressed as a function of E_T and a variable z, the ratio of the components of the two transverse energy vectors along the direction of one of the vectors: $z = -\vec{E}_{T1}.\vec{E}_{T2}/E_{T1}^2$. Therefore we compute a cross-section with the additional cut $z > z_{min} = 12\,\text{GeV}/E_{T1}$. In this case either photon can be photon '1', and therefore an event can contribute not at all, once or twice to the cross-section. In Table 5 we give the z values for our six events. Ten photons satisfy the z selection, which yields the following integrated cross-section:

$$\sigma_{\gamma\gamma} = 63 \pm 32 \pm 17 \text{ pb} \quad \text{for } E_{T\gamma 1} > 12\,\text{GeV},\ z > 12\,\text{GeV}/E_{T\gamma 1} \quad \text{and} \quad |\eta| < 3.$$

The QCD prediction (34 pb for the Born term and 54 pb for the full cross-section) is in good agreement with this result. Using the theoretical differential cross-section of reference [12], we transform the integrated cross-section to a value at one point in phase space. The result is:

$$\frac{E d^3\sigma_{\gamma\gamma}}{d^3p} = .0057 \pm .0029 \pm .0015 \text{ pb/GeV}^2 \text{ for } E_T = 20\,\text{GeV}, \quad z > 0.6 \quad \text{at } \eta = 0.$$

Summary

We have measured the cross-section for isolated direct photons in $p\bar{p}$ collisions at $\sqrt{s}$=546 GeV and $\sqrt{s}$=630 GeV. QCD predictions describe this cross-section well. The

photon-jet angular distribution is consistent with a $(1\text{-}\cos\theta^*)^{-1}$ law. The cross-section for two-photon production has been determined and is also well described by QCD predictions. The good agreement of our direct photon data with QCD is summarised in figure 6, where we also show direct photon data from the UA2 experiment [1] and the single jet cross-section, which is the origin of the π^0 background.

Acknowledgements

We are grateful to P. Aurenche, R. Baier, M. Fontannaz and D. Schiff for helpful discussions and providing the predictions adjusted to the experimental conditions of the present study. We are thankful to the management and staff of CERN and of all participating institutes for their vigorous support of the experiment. The following funding agencies have contributed to this programme:

Fonds zur Förderung der Wissenschaftlichen Forschung, Austria.
Valtion luonnontieteellinen toimikunta, Finland.
Institut National de physique nucléaire et de Physique des Particules and
Institut de Recherche Fondamentale (CEA), France.
Bundesministerium für Forschung und Technologie, Fed. Rep. Germany.
Istituo Nazionale di Fisica Nucleare, Italy.
Science and Engineering Research Council, United Kingdom.
Stichting Voor Fundamenteel Onderzoek der Materie, The Netherlands,
Department of Energy, USA.
The Natural Sciences and Engineering Research Council of Canada.

Thanks are also due to the following people who have worked with the collaboration in the preparations for and data collection on the runs described here: L. Baumard, F. Bernasconi, D. Brozzi, R. Conte, L. Dumps, G. Fetchenhauer, G. Gallay, J.C. Michelon and L. Pollet.

References

[1] A review of the experiments before 1984 is given by T. Ferbel and W.R. Molzon, Rev. Mod. Phys. **56** (1984) 181.
AFS Collaboration, Akesson et al., Phys. Lett. **158B** (1985) 282.
NA3 Collaboration, Badier et al., Z. Phys. C **31** (1986) 341.
UA2 Collaboration, J.A. Appel et al., Phys. Lett. **176B** (1986) 239.
WA70 Collaboration, Bonesini et al., preprint CERN-EP/87-222 (1987).
NA24 Collaboration, De Marzo et al., Phys. Rev. **D36** (1987) 8.

[2] UA1 Collaboration, G. Arnison et al., Phys. Lett. **122B** (1983) 102, **129B** (1983) 273, **134B** (1984) 469, **166B** (1986) 484, **193B** (1987) 389 and Europhys. Lett. **1** (1986) 327.

[3] B. Mours, Thesis at the Université de Savoie (France) (1988).

[4] F. Paige and S.D. Protopopescu: ISAJET program, BBNL 38034 (1986).

[5] UA1 Collaboration, 'Studies of the W and Z^0 properties at the CERN Super-Proton Synchrotron Collider', paper in preparation.

[6] R. Brun et al., GEANT3, CERN, DD/EE/84-1 (1984).

[7] P. Aurenche, R. Baier, M. Fontannaz, D. Schiff, Nucl. Phys. **B297** (1988) 661,

[8] D.W. Duke and J.F. Owens, Phys. Rev. **D30** (1984) 49.

[9] P.M. Stevenson, and H. Politzer, Nucl. Phys. **B277** (1986) 758.

[10] UA1 Collaboration, G. Arnison et al., Phys. Lett. **132B** (1983) 214.

[11] UA1 Collaboration, G. Arnison et al., Phys. Lett. **177B** (1986) 244.

[12] P. Aurenche et al., Z. Phys. **C29** (1985) 459.

[13] UA1 Collaboration, G. Arnison et al., Phys. Lett. **172B** (1986) 461.

Table 1: Luminosity and trigger selection criteria

Year	L	1^{st}level trigger threshold	2^{nd}level trigger threshold	Off − line threshold
Single photon				
1983	118 nb^{-1}	10 GeV	12 GeV	16 GeV
1984	259 nb^{-1}	10 GeV	15 GeV	20 GeV
1985	308 nb^{-1}	10 GeV	10 GeV	16 GeV
Two photon				
1984	186 nb^{-1}	6 GeV	8 GeV	12 GeV
	73 nb^{-1}	6 and 8 GeV	8 GeV	12 GeV
1985	308 nb^{-1}	6 GeV	7 GeV	12 GeV

Table 2: Percentage of direct photons (F_γ). Systematic errors take into account uncertainties in the determination of the expected distributions for π^0 and direct photon events.

Variable	$0 < \|\eta\| < 0.8$	$0.8 < \|\eta\| < 1.4$	$1.6 < \|\eta\| < 3$
F_γ for $\sqrt{s} = 546$ GeV			
E_c	$42 \pm 8 \pm 6$	$65 \pm 13 \pm 13$	$34 \pm 12 \pm 18$
E_r	$60 \pm 10 \pm 13$	$42 \pm 14 \pm 6$	$23 \pm 11 \pm 13$
S_1/E	$76 \pm 12 \pm 27$	$77 \pm 17 \pm 20$	$21 \pm 11 \pm 13$
L_γ	$47 \pm 7 \pm 9$	$48 \pm 11 \pm 12$	$33 \pm 9 \pm 12$
F_γ for $\sqrt{s} = 630$ GeV			
E_c	$42 \pm 3 \pm 6$	$32 \pm 6 \pm 7$	$28 \pm 6 \pm 15$
E_r	$45 \pm 4 \pm 10$	$44 \pm 6 \pm 7$	$27 \pm 5 \pm 15$
S_1/E	$29 \pm 4 \pm 11$	$41 \pm 7 \pm 11$	$13 \pm 5 \pm 9$
L_γ	$40 \pm 2.5 \pm 7$	$38 \pm 4 \pm 10$	$25 \pm 5 \pm 9$

Table 3: Cross-section for isolated direct photon production

E_T [GeV]	$Ed^3\sigma/d^3p$ $[pb/GeV^2]$ $(630GeV)$	$Ed^3\sigma/d^3p$ $[pb/GeV^2]$ $(546GeV)$
	$\eta = 0$	
17.	$6.42 \pm 0.57 \pm 1.12$	$3.91 \pm 0.37 \pm 0.44$
19.	$3.30 \pm 0.33 \pm 0.52$	$1.74 \pm 0.24 \pm 0.17$
21.	$1.54 \pm 0.20 \pm 0.22$	$1.12 \pm 0.19 \pm 0.10$
23.	$0.74 \pm 0.07 \pm 0.09$	
25.	$0.50 \pm 0.05 \pm 0.06$	$0.38 \pm 0.06 \pm 0.03$
27.	$0.381 \pm 0.047 \pm 0.038$	
29.	$0.246 \pm 0.037 \pm 0.022$	
31.5	$0.123 \pm 0.021 \pm 0.010$	
34.5	$0.056 \pm 0.014 \pm 0.004$	$0.049 \pm 0.013 \pm 0.002$
37.5	$0.051 \pm 0.013 \pm 0.003$	
40.5	$0.030 \pm 0.010 \pm 0.002$	
46.	$0.0111 \pm 0.0035 \pm 0.0004$	$0.0084 \pm 0.0060 \pm 0.0002$
55.	$0.0039 \pm 0.0018 \pm 0.0001$	
65.	$0.0037 \pm 0.0016 \pm 0.0000$	
75.	$0.0013 \pm 0.0009 \pm 0.0000$	
90.	$0.0002 \pm 0.0002 \pm 0.0000$	
	$\eta = 1.1$	
17.	$3.98 \pm 0.49 \pm 0.73$	$2.42 \pm 0.32 \pm 0.35$
19.	$1.97 \pm 0.27 \pm 0.34$	$1.47 \pm 0.24 \pm 0.20$
21.	$1.00 \pm 0.13 \pm 0.17$	$0.82 \pm 0.17 \pm 0.11$
23.	$0.52 \pm 0.06 \pm 0.09$	
25.	$0.397 \pm 0.049 \pm 0.065$	$0.231 \pm 0.048 \pm 0.029$
27.	$0.201 \pm 0.034 \pm 0.033$	
31.	$0.073 \pm 0.011 \pm 0.012$	
37.	$0.025 \pm 0.006 \pm 0.005$	$0.0113 \pm 0.0046 \pm 0.0015$
45.	$0.0052 \pm 0.0020 \pm 0.0010$	
60.	$0.0005 \pm 0.0003 \pm 0.0001$	
	$\eta = 2.3$	
16.5	$0.88 \pm 0.07 \pm 0.32$	$0.75 \pm 0.13 \pm 0.23$
17.5	$0.67 \pm 0.06 \pm 0.24$	
18.5	$0.47 \pm 0.05 \pm 0.17$	$0.36 \pm 0.05 \pm 0.10$
19.5	$0.26 \pm 0.03 \pm 0.09$	
20.5	$0.20 \pm 0.03 \pm 0.07$	
21.5	$0.151 \pm 0.024 \pm 0.052$	$0.125 \pm 0.026 \pm 0.035$
22.5	$0.115 \pm 0.020 \pm 0.040$	
23.5	$0.053 \pm 0.013 \pm 0.018$	
24.5	$0.050 \pm 0.012 \pm 0.017$	$0.038 \pm 0.013 \pm 0.010$
25.5	$0.020 \pm 0.008 \pm 0.007$	
28.	$0.0098 \pm 0.0024 \pm 0.0035$	
32.	$0.0028 \pm 0.0011 \pm 0.0011$	$0.0017 \pm 0.0006 \pm 0.0005$
37.	$0.0003 \pm 0.0002 \pm 0.0001$	

Table 4: parameters of two-photon events.

event	$E_{T\gamma 1}, E_{T\gamma 2}$[GeV]	$\eta_{\gamma 1}, \eta_{\gamma 2}$	$L_{\gamma 1}, L_{\gamma 2}$	$M_{\gamma\gamma}[GeV]$	$\lvert\phi_1 - \phi_2\rvert$
A	23.3, 22.7	1.2, 0.1	1.4, 3.1	53.2	180^0
B	31.7, 30.4	2.0, 1.0	0.5, 0.5	68.6	178^0
C	14.8, 12.0	1.7, −0.6	0.5, 1.8	48.1	171^0
D	13.9, 13.2	−0.4, −1.1	0.3, 1.8	28.0	155^0
E	18.7, 15.4	−0.9, −0.3	1.5, 1.5	35.3	174^0
F	14.0, 12.6	−2.6, .3	1.8, 0.3	58.0	174^0

Table 5: z values for two-photon events. z is the transverse energy balance parameter between the two photons, and defined by $z = -\vec{E}_{T1}.\vec{E}_{T2}/E_{T1}^2$

event	z_1	z_{1min}	z_2	z_{2min}
A	0.972	0.514	1.029	0.529
B	0.959	0.379	1.042	0.395
C	0.805	0.813	1.213	0.909
D	0.861	0.865	0.951	0.909
E	0.818	0.641	1.210	0.780
F	0.892	0.856	1.110	0.955

Figure captions

Fig. 1 $E_c, E_r, S_1/E, L_\gamma$ distributions for photon candidates with $E_T > 20$ GeV and $|\eta| < 0.8$ (1353 events). The solid line is the sum of the direct photon contribution (dashed line) and the π^0 contribution (dash-dotted line).

Fig. 2 Fraction of direct photons in the final sample, F_γ, as a function of E_T. The solid line is a fit of the points. The dashed areas represent the systematic uncertainties on F_γ.

Fig. 3 Isolated single photon cross-section. The dashed lines are the full order α_s^2 QCD cross-section predictions [7]. The full lines are the cross-section for isolated direct photons where we exclude all quark photon bremsstrahlung with quark-photon angle less than one radian.

Fig. 4 Azimuthal angle difference between jet and photon.

Fig. 5 Ratio of $cos\theta^*$ distributions for π^0 enriched sample to single photon enriched sample for events with $|\eta| < 0.8$. The solid line is the prediction using the $(1\text{-}cos\theta^*)^{-1}$ law for direct photon, and the $(1\text{-}cos\theta^*)^{-2}$ law for π^0 and taking into account the residual contaminations in both samples.

Fig. 6 Jet, single photon and two photon cross-sections. The jet cross-section is measured by UA1 [13]. There is an overall systematic error of 23% for single direct photon and 70% for jet cross-section. The solid lines are QCD predictions from Aurenche et al. [7] for direct photons and from J. Stirling scaled by 1.5 for jet cross-section.

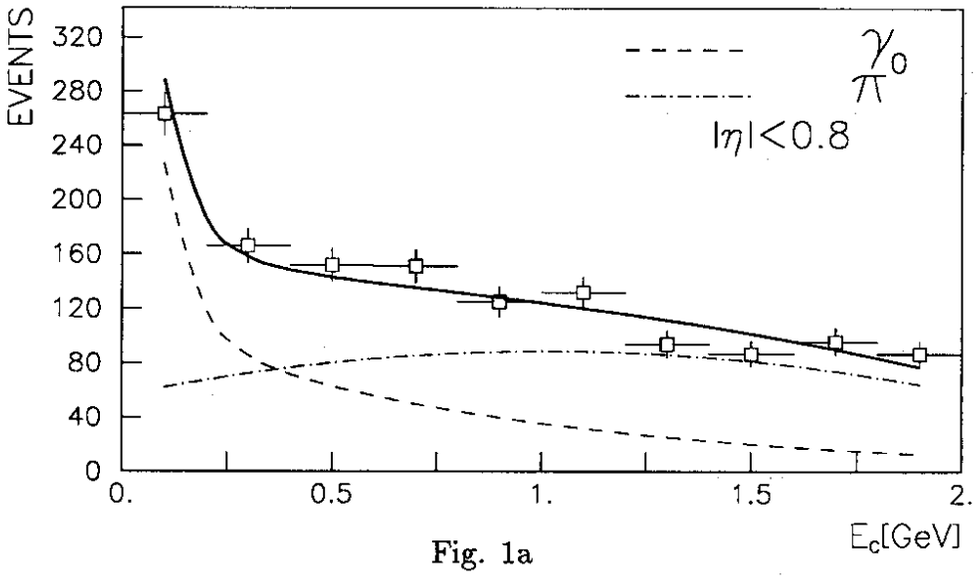
EVENTS
320
280
240
200
160
120
80
40
0
0.
0.5
1.
1.5
2.
E_c[GeV]
γ_0
π
$|\eta|<0.8$

Fig. 1a

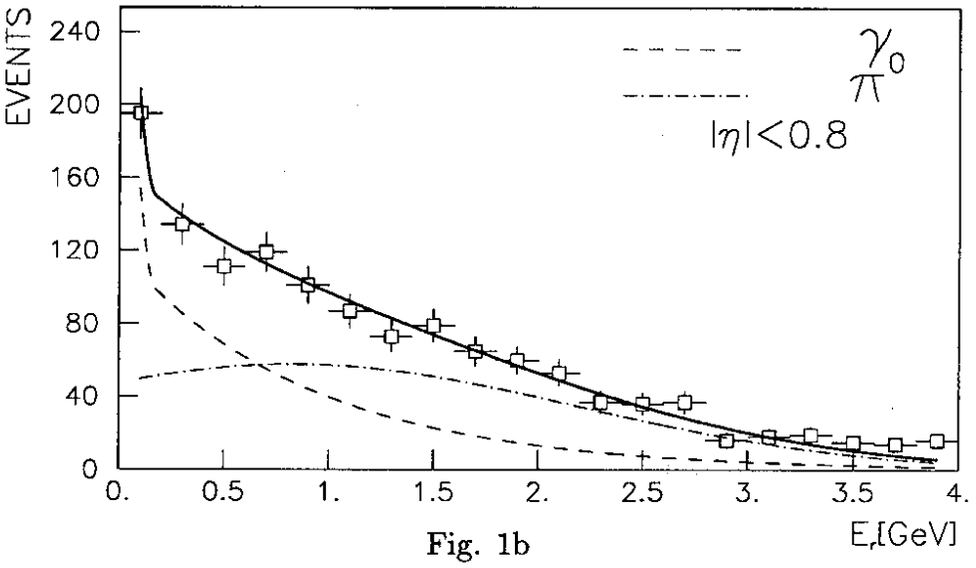
EVENTS
240
200
160
120
80
40
0
0.
0.5
1.
1.5
2.
2.5
3.
3.5
4.
E_γ[GeV]
γ_0
π
$|\eta|<0.8$

Fig. 1b

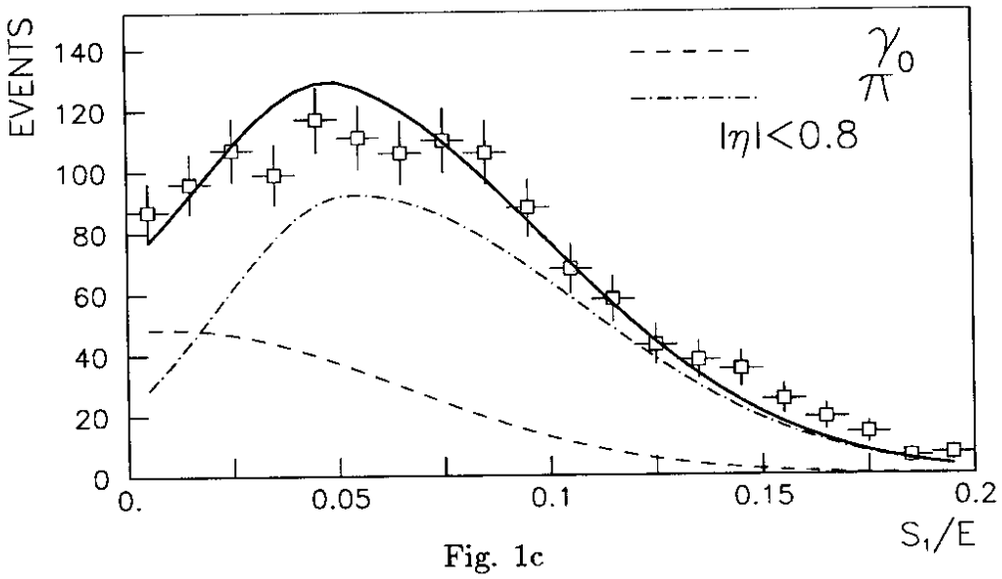
EVENTS
140
120
100
80
60
40
20
0
0.
0.05
0.1
0.15
0.2
S_1/E
γ_0
π
$|\eta|<0.8$

Fig. 1c

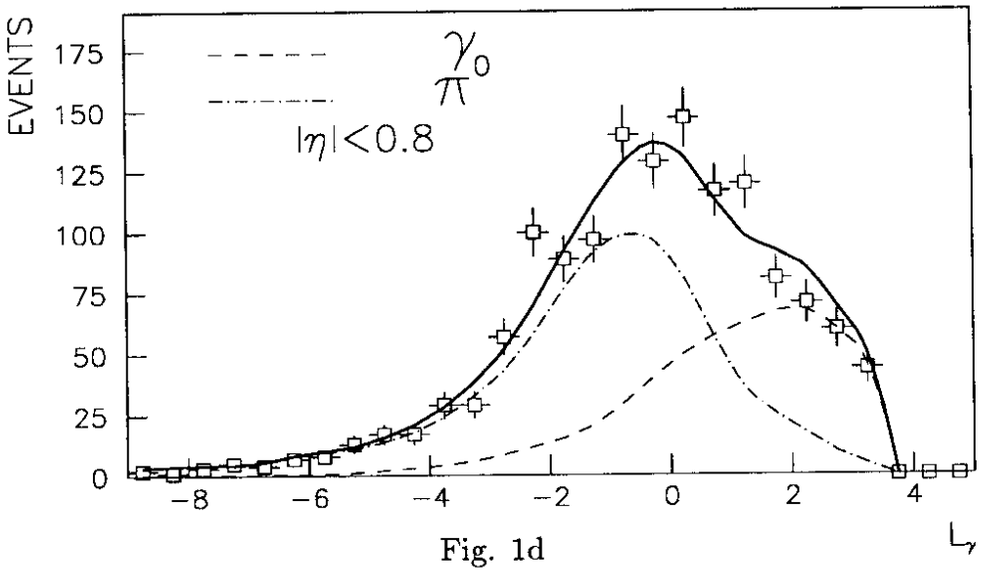
EVENTS
175
150
125
100
75
50
25
0
−8
−6
−4
−2
0
2
4
L_γ
γ_0
π
$|\eta|<0.8$

Fig. 1d

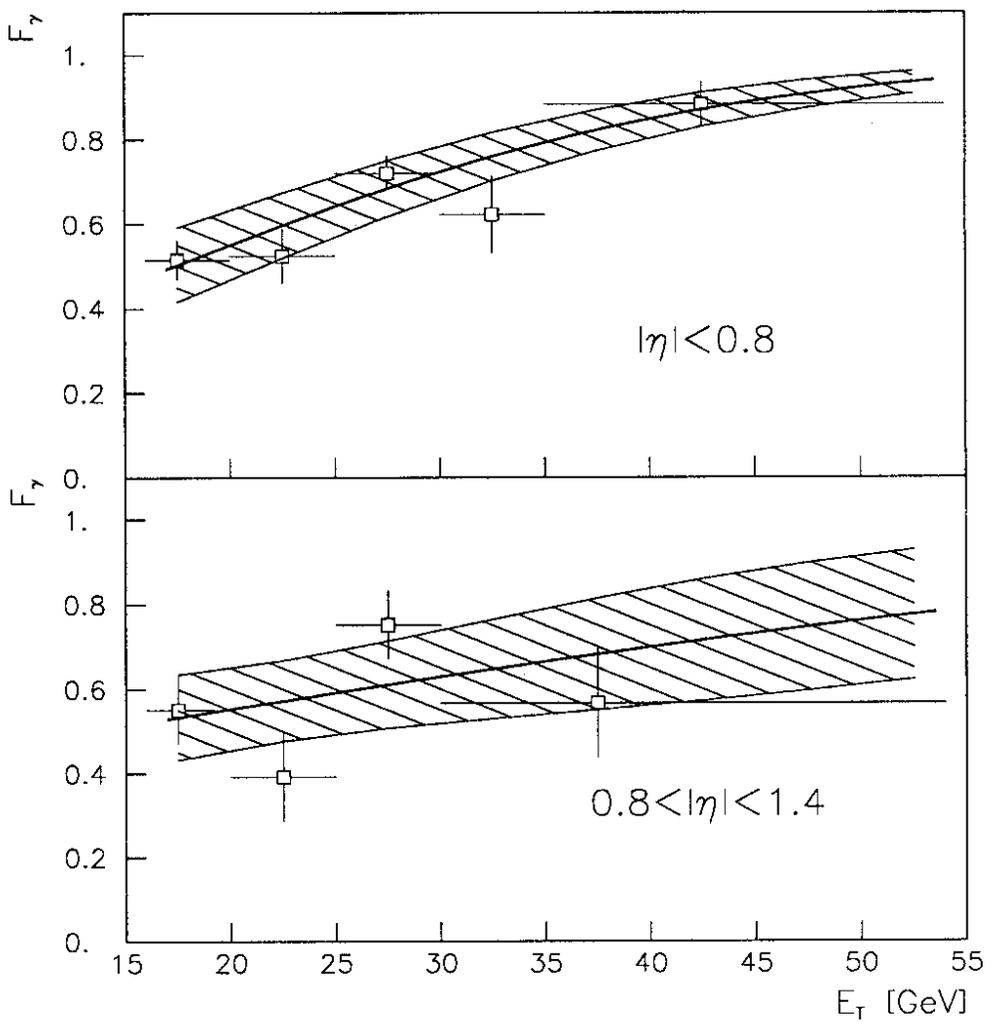
F_γ
1.
0.8
0.6
0.4
0.2
0.
$|\eta|<0.8$
F_γ
1.
0.8
0.6
0.4
0.2
0.
$0.8<|\eta|<1.4$
15
20
25
30
35
40
45
50
55
E_T [GeV]

Fig. 2

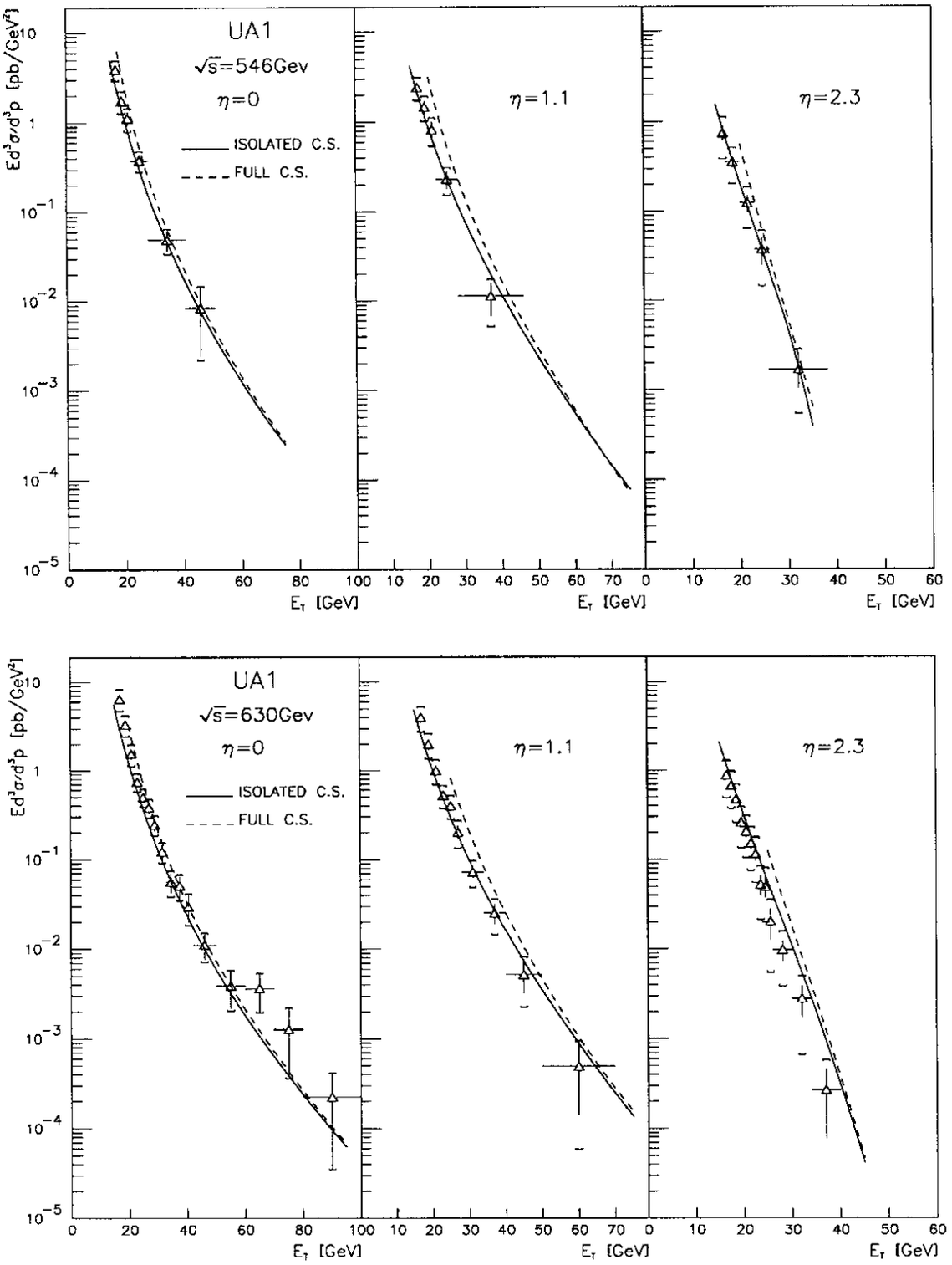
UA1
√s=546Gev
η=0
ISOLATED C.S.
FULL C.S.
η=1.1
η=2.3
Ed³σ/d³p [pb/GeV²]
E_T [GeV]
UA1
√s=630Gev
η=0
ISOLATED C.S.
FULL C.S.
η=1.1
η=2.3
Ed³σ/d³p [pb/GeV²]
E_T [GeV]

Fig. 3

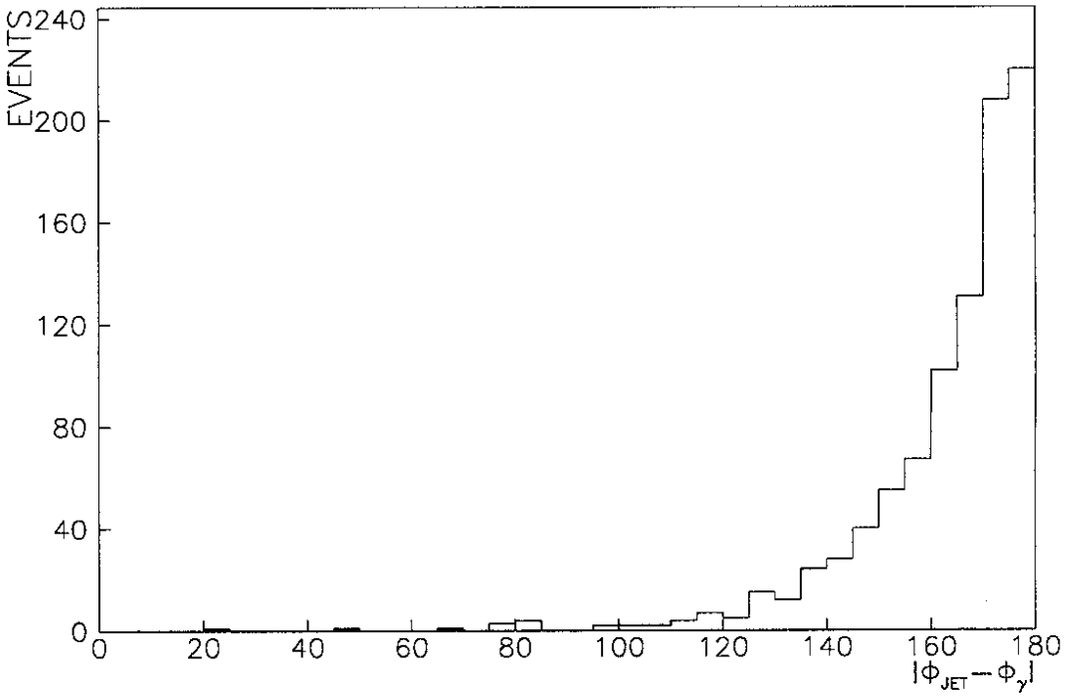
EVENTS
240
200
160
120
80
40
0
0
20
40
60
80
100
120
140
160
180
$|\Phi_{JET} - \Phi_\gamma|$

Fig. 4

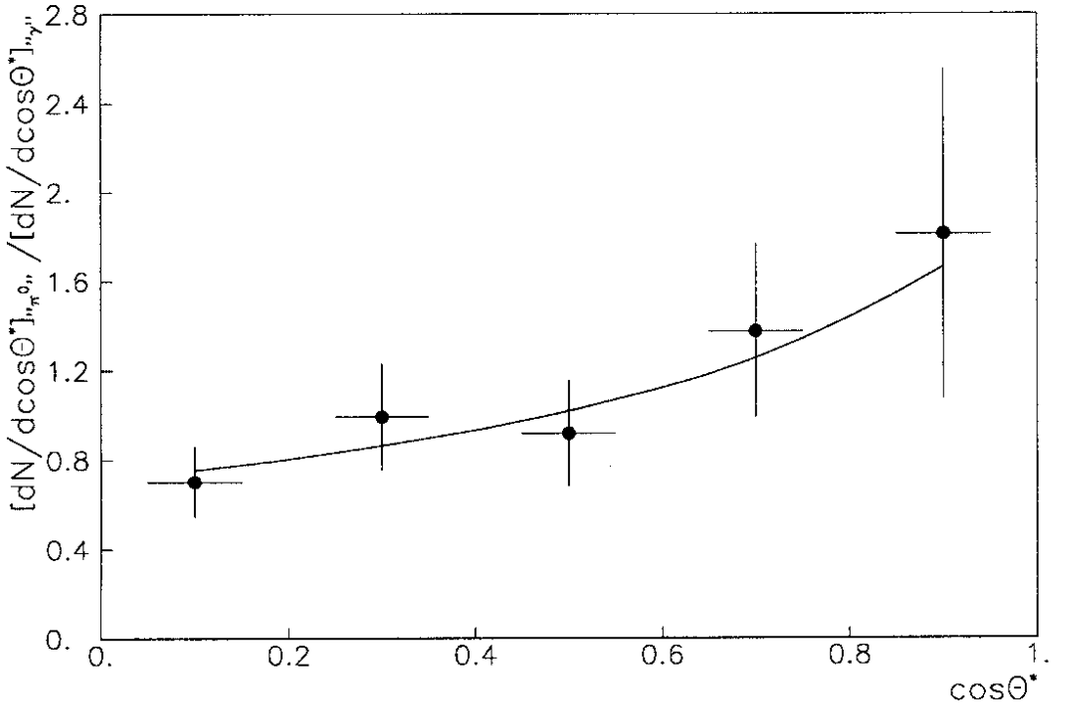
$[dN/d\cos\Theta^*]_{\pi^0}$ / $[dN/d\cos\Theta^*]_\gamma$
2.8
2.4
2.
1.6
1.2
0.8
0.4
0.
0.
0.2
0.4
0.6
0.8
1.
$\cos\Theta^*$

Fig. 5

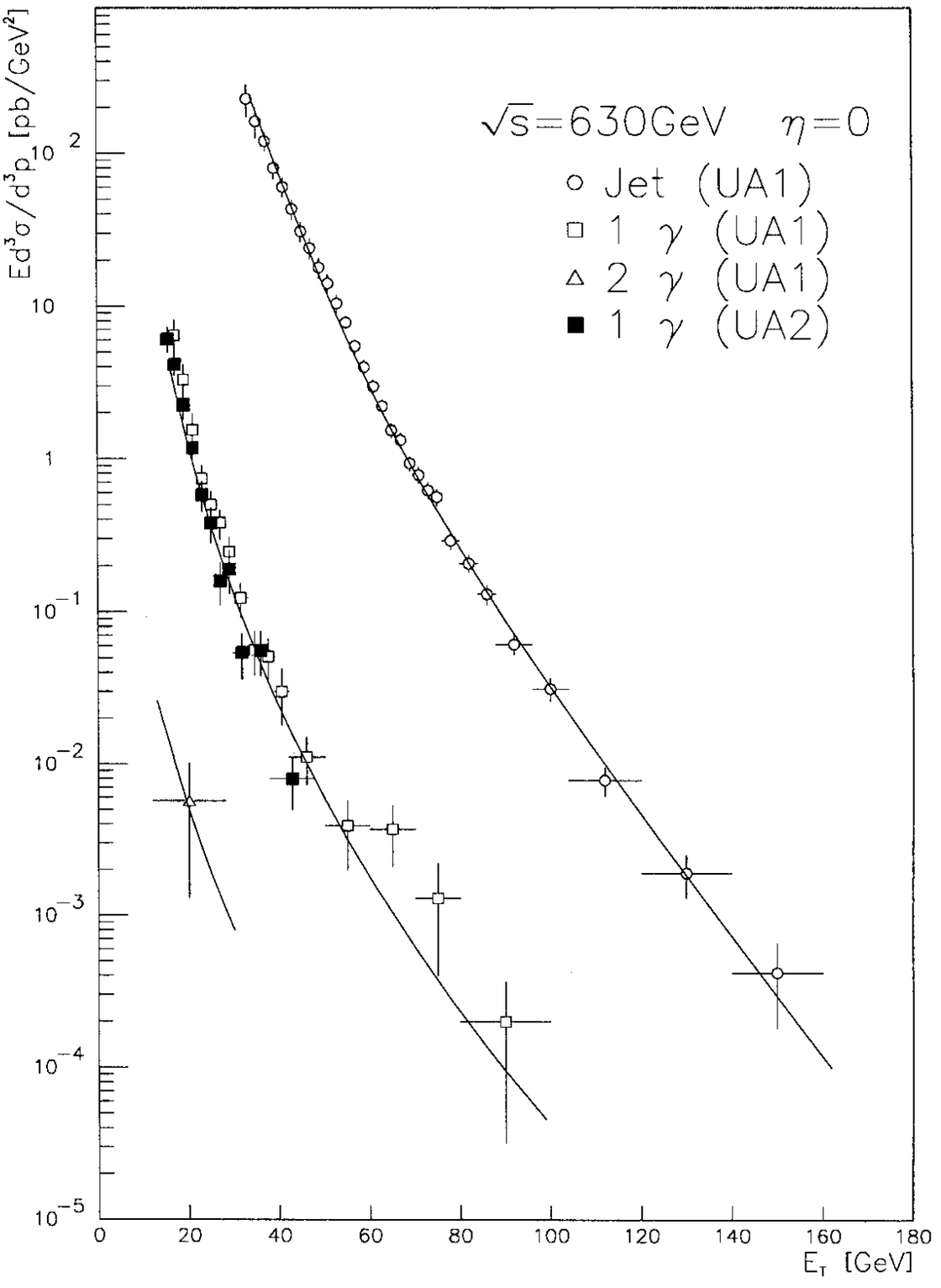
$\sqrt{s}$=630GeV η=0
Jet (UA1)
1 γ (UA1)
2 γ (UA1)
1 γ (UA2)
$Ed^3\sigma/d^3p$ [pb/GeV^2]
E_T [GeV]

Fig. 6